ACS APPLIED MATERIALS & INTERFACES

RESEARCH ARTICLE

www.acsami.org

Photodegradation of Methyl Orange under Visible Light by Micro-Nano Hierarchical Cu_2O Structure Fabricated by Hybrid Laser Processing and Chemical Dealloying

Changsheng Dong,[†] Minlin Zhong,[*,†] Ting Huang,[†] Mingxing Ma,[†] Dirk Wortmann,[‡] Mihael Brajdic,[‡] and Ingomar Kelbassa[‡]

[†]Key Laboratory for Advanced Material Processing Technology, Ministry of Education, Department of Mechanical Engineering, Tsinghua University, Beijing 100084, P. R. China

[‡]Fraunhofer Institute for Laser Technology ILT, RWTH Aachen University, Steinbachstrasse 15, 52074 Aachen, Germany

ABSTRACT: Micro-nano hierarchical structure on the substrate was fabricated by a hybrid approach including laser deposition, laser ablation and chemical dealloying. The structure consists of micro bumps with a width of 50 μm and a height of 100 μm, and nanoporous structures with a size of 70−150 nm on the micro bumps. XRD and XPS results confirm that these hierarchical structures were made of Cu_2O. For use in comparison, three additional structures with feature size in milliscale, microscale, and nanoscale were also prepared respectively by the proposed methods. Under visible light, the micro-nano structure exhibited the best performance of photodegradation. It is the result of the large specific surface and the catalytic reaction driven by the cuprous oxides.

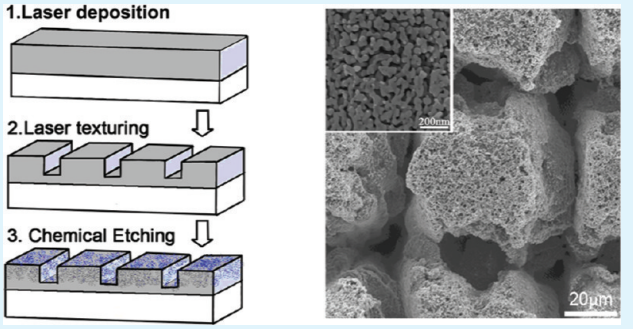

KEYWORDS: micro-nano hierarchical structure, photo degradation, laser ablation, dealloying

1. INTRODUCTION

Photocatalysis, the acceleration of a photoreaction in presence of a catalyst, depends on the ability of the catalysts to generate free radicals when creating electron−hole pairs. Currently photo catalysts, such as α-Fe_2O_3 nanoparticles, ZnO nanoparticles, and TiO_2, have been used to degrade and mineralize organic waste in water.[1−3] However, most of the photocatalysts can be excited only by UV light because of their wide band gap. To widen their practical applications, specifically to outdoor use, it is considered that photocatalysts, which can be activated under visible light, are indispensable. As an important p-type semiconductor material, Cu_2O has recently generated attentions because of its promising applications in many areas, such as solar energy conversion, gas sensor, and batteries.[4−6] Cu_2O is a p-type semiconductor, which is inexpensive and abundantly available. It has a direct band gap of 2.0 eV and a high optical absorption coefficient, and its theoretical solar cell conversion efficiency is greater than 13%.[7−9] The energy difference between the top valence and the first excited conduction sub-band of Cu_2O exhibits a blue shift as the Cu_2O film thickness decreases, which means that the nanostructure Cu_2O can be easily excited.[10] It is proven that the morphological and structural features of materials strongly affect their photocatalysis. Because of the high surface area, tunable pore size, and adjustable framework, micro- and nanostructures are exceptionally useful in catalysis.

Many approaches have been proposed to fabricate the micro- and nanostructures improving the catalysis, including lithographic patterning, chemical vapor deposition, sol−gel process, electrodeposition, hydro-gels process, aero-gels process, and plasma fluorination.[11−15]

Regarding microstructures, most conventional methods were used on organic materials in the microelectronic industry because of their difficult use on metal surfaces. Laser ablation has recently become a promising approach to fabricating thousands of periodic micro dimples or bumps on a metal surface.[16] The regular texturing can be conveniently designed and adjusted in comparison to random texturing used by other methods. For example, Lloyd fabricated periodic microstructures on the steel with an average periods ranging from 30 to 50 μm by utilizing a nano-second pulsed Nd:YVO_4 laser.[17] Herrmann produced bumps on metal surfaces with diameters of 230−250 μm and heights of 2−4 μm by using a picosecond Nd:YAG laser.[18]

As for nanostructures, dealloying is generally a useful approach to form bi-continuous nanostructures, in which one or more elements are chemically or electrochemically etched from a single-phase alloy matrix owing to the higher reactivity.[19,20] Erlebacher investigated the evolution of porosity in the dealloying process and pointed out four criterions, (1) the great difference in potential between the elements, (2) high content of less noble component, (3) homogeneous components with no phase separation, (4) fast

Received: July 29, 2011
Accepted: October 26, 2011
Published: October 26, 2011

diffusion of more noble atoms.[21] Compared to noble metals, such as Au−Ag, Cu−Mn alloy is less expensive, and the standard reversible potentials for Cu^{2+}/Cu and Mn^{2+}/Mn couples are 0.342 V (vs. Saturated Calomel Electrode SCE) and -1.135 V (vs. SCE) respectively, which preserves the high potential difference. In Au−Ag alloy, electro-deposition, sputtering and hammering were used to obtain the homogeneous components with refined structure.[22−24] The above methods are normally time consuming, and the application of the resulting films is restricted due to their thin thickness. However the depositions with a milliscale thickness and refined microstructure can be fabricated by laser deposition. They can be deposited on most metal substrates with metallurgy bonding. Furthermore, laser deposition can be time-saving. Therefore, laser deposition becomes a competitive method to fabricate the precursor for dealloying.

In the area of micro-nano hierarchical structures, scientists show great increasing interest in the production of inorganic materials containing regular frameworks with well-defined pore networks after the discovery of the superhydrophobic behavior. Currently, the morphology, size, and surface architecture of the micro-nano hierarchical structure can not be controlled separately,[25,26] particularly the microscale structure, which was a by-product due to clustering of nanostructures. The direct and controlled fabrication of hierarchical structures with micro- and nanostructures remains one of the key challenges.

In this study, we report a novel hybrid approach for fabricating a Cu surface with tunable micro-nano hierarchical periodical structures by continuous wave CO_2 laser depositing a copper−manganese alloy onto a substrate followed by a nanosecond pulsed Nd:YAG laser microtexturing and subsequent chemical dealloying for nanoporous structures. The regular micro and random nano hierarchical structures with large area are tunable by the laser processing and dealloying parameters. For means of comparison, three additional structures in milliscale, microscale, and nanoscale were formed by the same method respectively. These four scale surface structures demonstrate the photo degradation of methyl orange under visible light. Their degradation performance is compared and discussed.

2. EXPERIMENTAL PROCEDURES

Synthesis. The micro-nano hierarchical structure was prepared by a hybrid approach including laser deposition, laser ablation and chemical dealloying. Figure 1 schematically shows the preparing step: (1) Cu40Mn60 coatings deposited by laser; (2) microscale structure ablated by laser; (3) hierarchical structure adjusted by chemical dealloying. Firstly, the mild steel specimens of 200 mm × 50 mm × 15 mm were used as substrates. Cu and Mn powders with a diameter of 40-100 μm were used as raw materials. And Argon was used as protection gas and assistant gas. A PRC-3000 continuous wave CO_2 laser processing system was used for laser deposition. The Cu40Mn60 alloy precursor with a thickness of 0.5 mm and dimensions of 10× 10 mm was deposited by laser on the mild steel surface. The main processing parameters were list below: laser power ranging from 1100 to 1400 W, beam diameters of 2−4 mm, beam scanning velocities of 300−500 mm/min and powder feeding rates of 2−6 g/min. Secondly, the surface of the workpiece was machined and polished to remove scratches. A Powerlase diode pumped Nd:YAG laser was used to form regular microscale bumps on the deposited Cu40Mn60 coatings. The laser pulse repetition rate was 10 kHz and the spacing was 50 μm. Thirdly, the laser textured

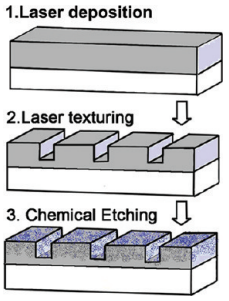

Figure 1. Fabrication process for the micro-nano hierarchical structure. (1) Laser deposition (2) Laser ablation (3) Chemical dealloying.

specimens were further immersed into a 0.05 M HCl aqueous solution at room temperature to obtain random nano-porous substructures on the micro-scale bumps. Thus the micro-nano hierarchical structures were achieved. The dealloyed specimens were rinsed into deionized water and ethanol at least five times to remove the residual chemical substances.

Characterization. The micro-nano hierarchical structures were examined under LEO-1530 scanning electron microscope (SEM) operated in secondary electron mode at 10 kV. A Talysurf5P-120 was employed for measuring the width and height of the bumps after laser ablation. A scanning white light interferometer was used to image and measure the microstructures and topography of the targets in an area of 0.6 mm × 0.8 mm. The results were taken at 3 different locations to obtain an accurate assessment. The X-ray diffraction (XRD) patterns of the specimen were recorded by a BRUKER D8 ADVANCE X-ray diffractometer using Cu Kα radiation. The detected diffraction angle (2θ) was scanned from 20 to 100° with a speed of 8°/min.

Evaluation of Photodegradation. The photo degradation measurements were performed in 5 mL of 10 mg/L methyl orange with various catalysts using an incandescent lamp for 4 h at 25 °C. The concentration of the methyl orange was tested after 1, 2, 3, and 4 h. The degradation process was monitored by an UV−vis absorbance spectrometer UV-2100 (measuring the transmission at 460 nm).

The photo degradation can be described by the Langmuir-Hinshelwood kinetics model (eq 1):[26]

$$v = -\frac{dC}{dt} = \frac{k_r K C_{eq}}{1 + K C_{eq}} \quad (1)$$

Where v is the rate of degradation, k_r is the apparent reaction rate constant, K is the absorption coefficient of the substance to be degraded and C_{eq} is the equilibrium concentration. For very low concentrations ($KC_{eq} \ll 1$), the Langmuir−Hinshelwood equation simplifies to a pseudo-first-order kinetic law (eq 2)

$$\ln\left(\frac{C_t}{C_0}\right) = -k_r K t \quad (2)$$

The degradation of the methyl orange was calculated according to its initial and final concentrations of the solutions by eq 3

$$D\% = \frac{(C_0 - C_t)}{C_0} \times 100\% \quad (3)$$

where D% is the degradation rate, C_0 is the initial transmission of methyl orange, and C_t is the transmission of methyl orange after 't' minutes. The reference sample of methyl orange was also detected under the same conditions because the methyl orange

can be decomposed via a mechanism of self-sensitization catalytic degradation under visible light illumination. To reflect the actual decomposition by the catalysts, the transition and photodegradation removes its self-degradation.

3. RESULTS

3.1. Surface Structures under Four Different Scales. Specimens with surface structures of four different scales (milliscale, microscale, nanoscale, and micro-nanoscale) were prepared and their photo degradation performances were compared.

Figure 2 shows the dendrite structure of the Cu40Mn60 coating after the laser deposition process. The second dendrite arm spacing is about 1.6 μm, which composes the fine microstructure. This matches well with the dealloying demands. For dealloying process, the milliscale specimen, 10 mm × 10 mm × 0.5 mm, was cut from the laser deposited coating specimen parallel to the surface, along the laser scanning direction. The milliscale specimen was then abraded on 2000 grit fine metallurgical paper for a smooth surface.

Figure 3a shows the surface morphology of the microscale bumps after the laser ablation. The laser textured surfaces are characterized as high-density microscale dimples/bumps. The spacing between the bumps is about 50 μm and the height is about 100 μm, detected by an interferometer (shown in Figure 3b). This indicated a uniform and regular microscale structure free of defects on the surface of the substrate. In fact, the spacing and the depth can be easily tuned by the scanning route of the pulsed laser and laser ablation parameters (the laser power, scanning speed, frequency, and pulse duration), respectively.

Figure 4 shows the SEM image of a random nanoscale porous structure. The structure is characterizing "sponge" morphology with the ligament width and spacing in the range of 70−120 nm. The specimen was immersed in 0.05 M HCl for 7 days to obtain nanoscale structure. During the dealloying process, the manganese reacts with HCl and thus is removed away. The nanoporous copper is formed in the diluted acid solution through the following reaction (eq 4)[20]

$$(\mathrm{Cu}, \gamma\mathrm{Mn}) + 2\mathrm{H}^{+} = \mathrm{Cu(fresh)} + \mathrm{Mn}^{2+} + \mathrm{H}_2 \qquad (4)$$

This structure has ultrahigh surface areas. The nanoporous size can be adjusted by the solution concentration and chemical dealloying time. Smaller nanoporous can be achieved by using the solution of lower concentration, longer dealloying time and a precursor composition with more copper.

Combining the above laser ablation and chemical dealloying process, the specimens with micro-nano hierarchical structure were fabricated as shown in Figure 5. A random nano-porous substructure on regular microscale bumps was obtained. The nanoporous structures can be observed at the bottom and top of

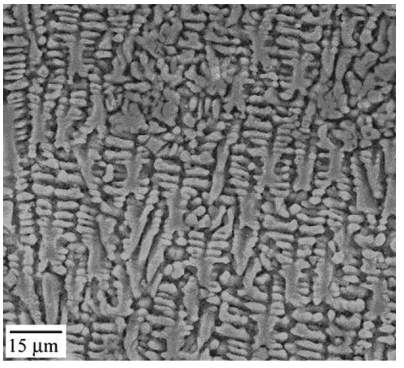

Figure 2. Microstructure of the Cu−Mn alloy coating deposited by laser.

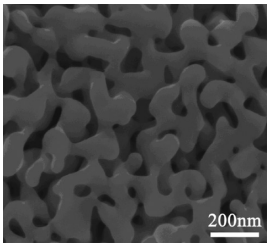

Figure 4. Nanostructure fabricated by chemical dealloying.

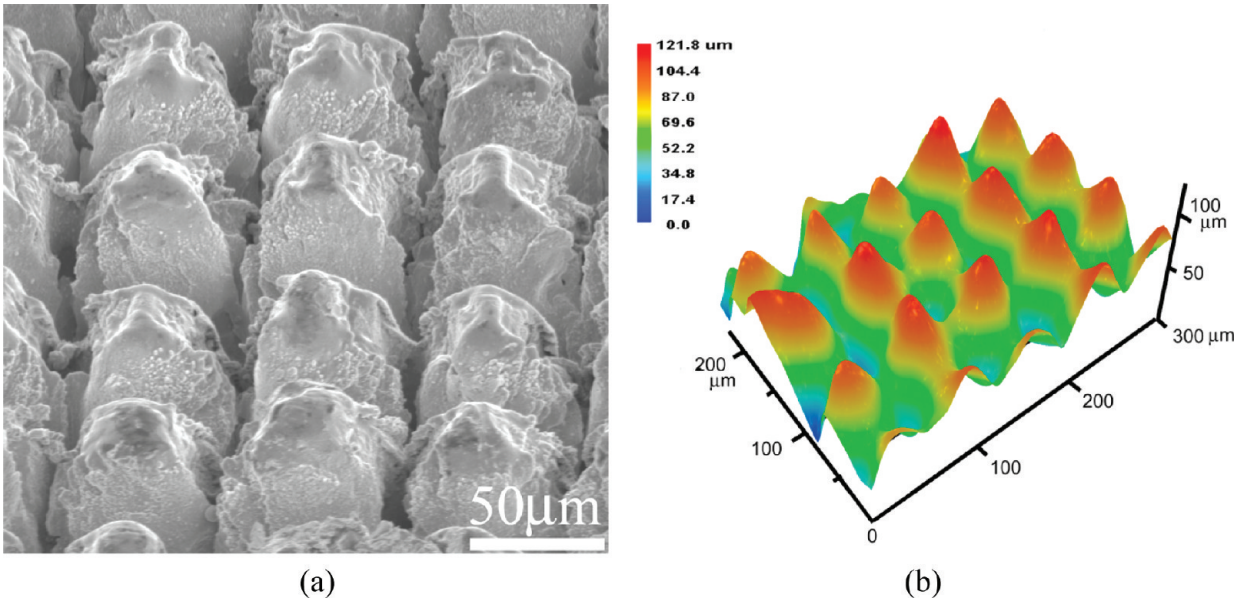

Figure 3. Microscale bumps ablated by laser: (a) SEM micrograph showing morphology of the bumps; (b) light interferometer result of the bumps.

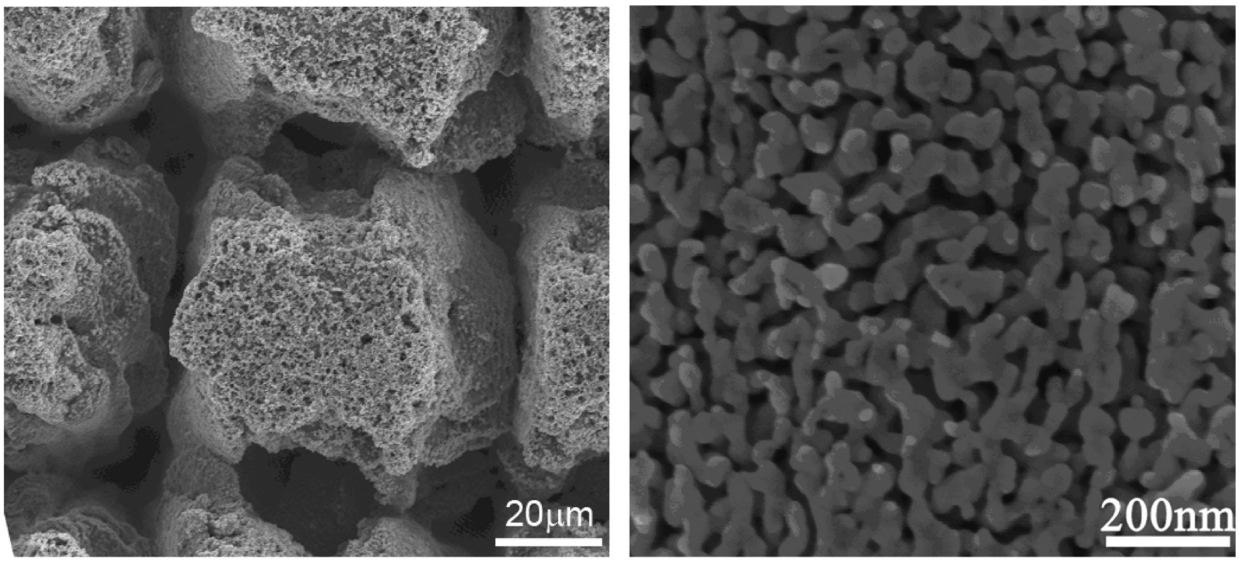

Figure 5. Hierarchical structure by laser ablation coupled with chemical dealloying: (a) the microscale bumps; (b) the nanoporous structure (magnification of a).

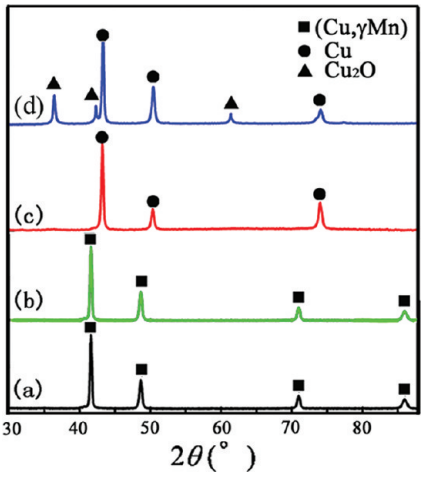

Figure 6. XRD patterns of (a) Cu−Mn alloy coating deposited by laser, (b) Cu−Mn alloy coating ablated by laser, (c) hierarchical structure by the hybrid method, (d) hierarchical structure under oxidation.

the textured microscale bumps. Because of the influence of the geometric curvatures of the micro-scale bumps, the dimension of the nanoporous structure at the bottom and the top of the textured bumps were slightly different. By comparing Figures 4 and 5b, it is clear that the ligament size in hierarchical structure is much smaller than its counterpart in nanostructure. This is because the microstructure becomes refined and the components become homogenous as the scanning speed of laser ablation increases. The similar phenomenon was also observed in our previous study.[19]

3.2. Composition and Phase of Various Structures. Figure 6 shows the X-ray diffraction (XRD) patterns of the above samples in different scales structure. The laser deposited Cu−Mn coating in milliscale is a single-phase alloy. Its diffraction peaks can be indexed as an fcc (Cu, γMn) phase with main diffraction peaks of (111), (200), and (220). As indicated by Erlebacher and his co-workers, single-phase alloys with homogeneous composition and fine microstructure is a precondition of nano-porosity during a dealloying process.[21] Because laser ablation process usually does not change the composition and phase, the specimen with micro-scale structure preserves the single (Cu, γMn) phase as demonstrated by identical diffraction peaks in the milliscale specimen of Figure 6b. After the chemical dealloying process, Mn is dissolved and nanoporous Cu forms. Figure 6c shows the diffraction patterns of the two specimens with nanoscale structures and micro-nano hierarchical structures. They displayed only the peaks of Cu phase by XRD, obviously different from those of the microscale or milliscale specimens. After the nanoporous Cu specimens (the nanoscale and the micro-nanoscale) were exposed to the air, the color of the nanoporous structures changes immediately to dark green because of oxidation. Peaks of Cu_2O appears in its XRD pattern (shown in Figure 6d), indicating that the oxidation occurs at the exterior of the structure, whereas the nanoporous Cu structure remains. The process of full oxidation from Cu to Cu_2O nanoporous structure took up a few hours, depending on the environmental conditions and nanoporous structure size. The oxidation can be regarded as an oxygen diffusion and lattice expansion process. As a result, the crystal structure and material changes from fcc Cu to Cu_2O with a corresponding lattice expansion. The generated Cu_2O is stable at room temperature, which could be confirmed by XRD pattern of samples aged for 7 days. This is contrary to conventional results. Generally, Cu^{2+} is more stable than Cu^{+} and copper is easier to be oxidized into CuO instead of Cu_2O. In order to further characterize the status of copper, X-ray photoemission spectroscopy (XPS) was used. The elements C, O, Cu of the samples detected by XPS are shown in Figure 7a. The intensities of the Cu peaks are affected by the oxide layer thickness and a contamination layer of carbon on top of the oxide. To measure the Cu2p core level as shown in Figure 7b, the spectrum of copper at wavelengths between 925 eV and 970 eV was investigated. There are two main Cu2p XPS peaks at 931.6 and 951.6 eV, which could be attributed to the Cu^{+} double peaks for Cu2p3/2 and Cu2p1/2

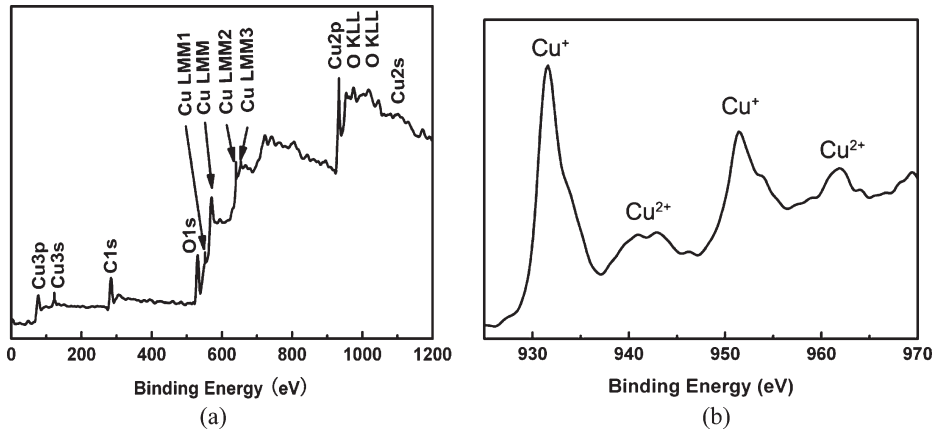

Figure 7. XPS survey spectrum of (a) the hierarchical structure, (b) Cu2p.

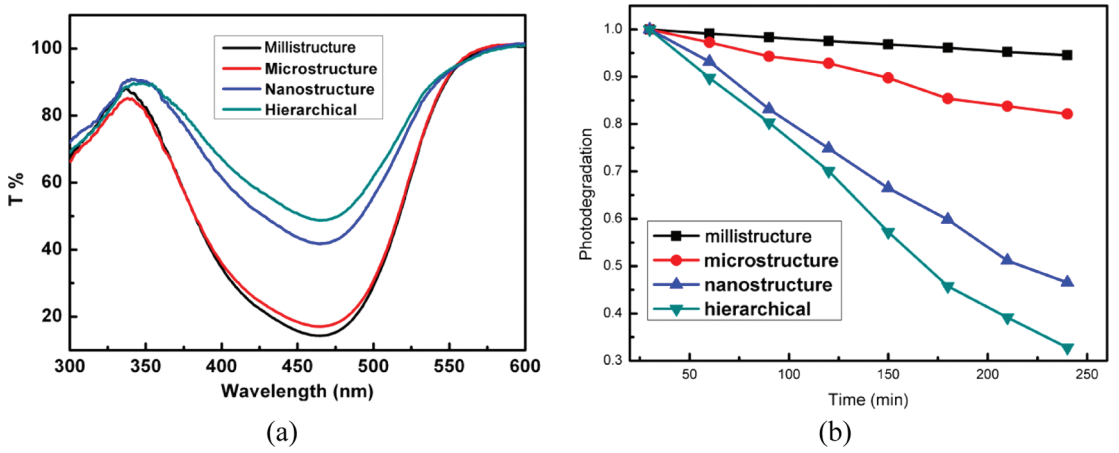

Figure 8. Photo degradation results: (a) transition of methyl orange; (b) photodegradation rate with the variation of time.

respectively. This confirms that the main composition of the hierarchical structure is Cu_2O. And there are two low Cu2p XPS peaks at 942 and 962 eV, attributed to the Cu^{2+} double peaks. The relatively low peaks imply a small amount of CuO on the surface of the specimen. In general, Cu_2O instead of CuO is the major component of the micro-nano hierarchical structure. With the use of XPS, Huang also reported that copper existed as Cu_2O in the nano particles while as CuO in the microparticles.[10] And Parlkar also pointed out that Cu_2O is more stable than CuO when the size of the particle is reduced to 25 nm. He postulated that an enhancement in the ionic character of the system and a consequent tendency to structures of comparatively higher symmetry were attributed to the reduction of the particle size.[27] Because Cu_2O has a higher symmetry structure than CuO (monoclinic), nano particles are more often achieved in Cu_2O. Besides, Yin also noted that there was a considerable energetic difference between the fcc structure (Cu) and the monoclinic structure (CuO), as atom rearrangement and lattice/unit cell reconstruction is required. This may help to explain why the transformation to crystalline CuO does not occur in these nano crystals, in addition to the possible stabilization of the oxidation state by the ligand shell.[28] All the above statement explained why Cu_2O is formed instead of CuO in our hierarchical structure.

3.3. Photodegradation in various structures. Figure 8a shows the transmission and visible light driven photo catalytic degradation of methyl orange by the four specimens (milliscale, microscale, nanoscale, and micro-nanoscale). The degradation by using these catalysts occurs from 300 nm to 550 nm, and the transmission peak is 460 nm, very near to the peak of sun radiation. This indicated that the degradation was under light irradiation. In addition, the transmission of the specimens with nanoscale structure and the hierarchical structure are obviously better than that of other two specimens due to the nanoscale structure. Figure 8(b) shows that the concentration of methyl orange in various scale structures decreases with time under visible light irradiation. After 4 h, the concentrations of methyl orange decrease to 32.77, 46.53, 82.11, and 94.54% for micro-nano hierarchical structure, nanoscale structure, microscale structure, and milliscale plate, respectively. Among those, the hierarchical structure displays the best result in photo degradation. The difference is mainly due to the various scale structures with different compositions. The specimens having intense absorption in the visible range can be attributed to the high photocatalytic activity of Cu_2O and dual scale structures under visible light irradiation.

4. DISCUSSION

Normally, the mechanism of degradation can be divided into two parts: adsorption process and catalytic reaction, which affect the transport and the fate of other organic and inorganic species.

Regarding adsorption, the large specific surface plays a dominant role since it can provide multiple areas of absorption. The degradation ratio of the specimen with microscale structure is merely 3 times than the specimen with the milliscale structure because the surface area is enlarged to 2 times by white light interferometer. The same result is also observed in the other two specimens. By the BET analysis, the specific surface is 8.634 and 9.603 m^2/g for nanoscale structure and hierarchical structure, respectively. As illustrated in the Figure 8, the specimen with hierarchical structure displayed a considerably larger extent of photo degradation reaction than the solid ones after irradiation, indicating that large specific surface improve the performance of the photo degradation.

As for the catalytic reaction, the holes and electrons are generated in the solid catalyst when the wavelength of the light corresponds to the absorption transition of the solid catalyst (eq 5). The holes (h^+) generated are highly oxidizing, and thus most compounds are essentially oxidized completely. The electrons can be scavenged by molecular oxygen O_2 to yield $O_2\cdot$ or H_2O_2 and $\cdot OH$ (as shown in eqs 6−10).[29,30] It is well known that $\cdot OH$ is a powerful oxidizing agent with a redox potential of 1.9 V, which can degrade most pollutants.[31] In the hierarchical structure, the composition changes with the structure refinement. Cuprous oxide (Cu_2O) becomes stable when the structure is reduced down to nano size, as previously demonstrated. Cuprous oxide (Cu_2O) is an important p-type semiconductor with a direct band gap of 2.0−2.2 eV, which can be used to driven photo catalysis directly for the degradation of organic contaminants.[7−9] Wu pointed out that Cu^+ promoted electron-hole generation due to the lower band gap,[32] and the existence of copper is beneficial in transferring photoinduced electrons and enhancing the separation efficiency of photoinduced electron−hole pairs, which can reduce the rate of charge-carrier recombination. Consequently, the rate of the primary interfacial charge transfer increases. What's more, the band edges shift to yield larger redox potentials when the dimension of a semiconductor particle falls below a critical radius.[33] The small size of the nano structure will lead to the improvement in photo catalytic activity.[34] Huang pointed out that the band gap of Cu_2O can be tuned by certain factors, such as particle size, not only making good use of visible light as photo catalysts but also being used as sensitized semiconductor for solar cells.[10] The band gap of cuprous oxides can be modified in the range of 1−2.2 eV by tuning the nano size, which promotes the photodegradation.[9] Therefore, the catalytic reaction becomes easier and more efficient.

$$h\nu(2.0\ \mathrm{eV}) + Cu_2O \rightleftharpoons h^+ + e^- \quad (5)$$

$$OH^- + h^+ \rightarrow HO^\bullet \quad (6)$$

$$H_2O + h^+ \rightarrow H^+ + HO^\bullet \quad (7)$$

$$O_2 + 2H_2O + 2e^- \rightarrow H_2O_2 + 2OH^- \quad (8)$$

$$Cu^{2+} + H_2O_2 \rightarrow Cu^+ + O_2^{\bullet -} + 2H^+ \quad (9)$$

$$Cu^+ + H_2O_2 \rightarrow Cu^{2+} + OH^- + HO^\bullet \quad (10)$$

In conclusion, the best performance of photo degradation in the hierarchical structure is attributed not only to the larger specific surface, but also to the catalytic reaction driven by the cuprous oxides.

5. CONCLUSION

The micro-nano hierarchical structure of Cu_2O on copper substrate was fabricated by a hybrid approach combining laser deposition, laser ablation, and chemical dealloying. The microbumps with a width of 50 μm and a height of 100 μm were fabricated by laser ablation, and the nanoporous structures with a size of 70−150 nm on the above mentioned microbumps were formed by chemical dealloying. The hierarchical structure exhibits the best performance of photodegradation of methyl orange. The photo degradation ratio reaches 68% after 4 h irradiation under the visible light. It is the result of the large specific surface and the catalytic reaction driven by the cuprous oxides. This widens the applications of the photodegradation under the visible irradiation.

AUTHOR INFORMATION

Corresponding Author
*E-mail: zhml@tsinghua.edu.cn.

ACKNOWLEDGMENT

This was was supported by National Natural Science Foundation of China (90923021), Independent Scientific Research Plan of Tsinghua University (2010THZ0), and Key Program for Science and Technology Project of Beijing Municipal Education Commission (KZ201110005001).

REFERENCES

(1) Ahmad, U.; Abaker, M.; Faisal, M.; Hwang, S.W.; Baskoutas, S.; Al-Sayari, S.A. *J. Nanosci. Nanotechnol.* **2011**, *4*, 3474–3480.
(2) Xu, T. G.; Zhang, L. W.; Cheng, H. Y.; Zhu, Y. F. *Appl. Catal. B* **2011**, *101*, 382–387.
(3) Varley, J. B.; Janotti, A. J.; Vandewalle, G. C. *Adv. Mater.* **2011**, *23*, 2343–2347.
(4) Li, X.; Gao, H.; Murphy, C. J.; Gou, L. *Nano Lett.* **2004**, *4*, 1903–1907.
(5) Guan, L.; Pang, H.; Wang, J. J.; Lu, Q. Y.; Yin, J. Z.; Gao, F. *Chem. Commun.* **2010**, *46*, 7022–7024.
(6) Zhang, J. Y.; Zhu, H. L.; Zheng, S. K.; Pan, F.; Wang, T. M. *ACS Appl. Mater. Inter.* **2009**, *1*, 2111–2114.
(7) Yu, Y.; Du, F. P.; Yu, J.C.; Zhuang, Y. Y.; Wong, P. K. *J Solid State Chem.* **2004**, *177*, 4640–4647.
(8) Hung, L.; Tsung, C. K.; Huang, W. Y.; Yang, P. D. *Adv. Mater.* **2010**, *22*, 1910–1914.
(9) Poulopoulos, P.; Baskoutas, S.; Pappas, S. D.; Garoufalis, C. S.; Droulias, S. A.; Zamani, A.; Kapaklis, V. *J. Phys. Chem. C* **2011**, *115*, 14839–14843.
(10) Huang, J. F.; Sun, I. W. *Adv. Funct. Mater.* **2005**, *15*, 989–994.
(11) Paxton, W. F.; Spruell, J. M.; Stoddart, J. F. *J. Am. Chem. Soc.* **2009**, *131*, 6692–6694.
(12) Kuo, C.; Tseng, Y.; Yuan, Y. *Chem. Lett.* **2006**, *35*, 356–357.
(13) Byeon, J. H.; Kim, J. W. *ACS Appl. Mater. Interfaces* **2010**, *2*, 947–951.
(14) Bigall, N. C.; Herrmann, A. K.; Vogel, M.; Rose, M; Simon, P.; Wilder, C. C.; Dorfs, D.; Kaskel, S.; Gaponik, N.; Eychmuller, A. *Angew. Chem., Int. Ed.* **2009**, *48*, 9731–9734.
(15) Liu, R.; Liu, J. F.; Yu, S. J.; Liu, Q.; Jiang, G. B. *Chem. Commun.* **2011**, *47*, 1613–1615.
(16) Nayak, B. K.; Gupta, M. C. *Opt. Laser Eng.* **2010**, *48*, 940–949.
(17) Lloyd, R.; Abdolvand, A.; Schmidt, M.; Crouse, P.; Whitehead, D.; Liu, Z.; Li, L. *Appl. Phys. A* **2008**, *93*, 117–122.
(18) Herrmann, T.; Haloui, H.; Knappe, R.; Henrich, B.; Nebel, A. In *ICALEO 2006−25th International Congress on Applications of Laser*

and Electro-Optics; Scottsdale, AZ; Laser Institute of America: Orlando, FL, 2006; pp 304−310.
(19) Dong, C. S.; Gu, Y.; Zhong, M. L.; Li, L.; Sezer, M.; Ma, M. X.; Liu, W. J. *J. Mater Process Tech.* **2011**, *211*, 1234–1238.
(20) Chen, L.Y.; Yu, J. S.; Fujita, T.; Chen, M. W. *Adv. Funct. Mater.* **2009**, *19*, 1221–1226.
(21) Erlebacher, J.; Aziz, M. J.; Karma, A.; Dimitrov, N.; Sieradzki, K. *Nature* **2001**, *410*, 450–453.
(22) Ding, Y.; Kim, Y. J.; Erlebacher, J. *Adv. Mater.* **2004**, *16*, 1897–1900.
(23) Kim, H; Kim, Y.; Joo, J. B.; Ko, J. W.; Yi, J. *Microporous Mesoporous Mater.* **2009**, *122*, 283–287.
(24) Okman, O.; Lee, D. Y.; Kysar, J. W. *Scr. Mater.* **2010**, *63*, 1005–1008.
(25) Yan, C. L.; Xue, D. F. *J. Phys. Chem. B* **2006**, *110*, 11076–11080.
(26) Kim, S. B.; Hong, S. C. *Appl. Catal. B.* **2002**, *35*, 305–315.
(27) Palkar, V. R.; Ayyub, P.; Chattopadhyay, S.; Multani, M. *Phys. Rev. B* **1996**, *53*, 2167–2170.
(28) Yin, M.; Wu, C. K.; Lou, Y.; Burda, C.; Koberstein, J. T.; Zhu, Y.; O'Brien, S. *J Am. Chem. Soc.* **2005**, *127*, 9506–9511.
(29) Arana, J.; Fernandez, R. C.; Gonzalez, D. O.; Herrera, M. J. A.; Perez, P. J. *Catal Today.* **2005**, *101*, 261–266.
(30) Liu, Y.; Liu, R.; Liu, C.; Luo, S.; Yang, L.; Sui, F.; Teng, Y.; Yang, R.; Cai, Q. *J Hazard Mater.* **2010**, *182*, 912–918.
(31) Huang, L.; Peng, F.; Yu, H.; Wang, H. *Solid State Sci.* **2009**, *11*, 129–138.
(32) Wu, Y.; Lu, G.; Li, S. *Catal. Lett.* **2009**, *133*, 97–105.
(33) Hoffmann, M. R.; Martin, S. T.; Choi, W.; Bahnemann, D. W. *Chem. Rev.* **1995**, *95*, 69–96.
(34) Xu, H.; Wang, W.; Zhu, W. *J. Phys. Chem. B* **2006**, *110*, 13829–13834.